Migrating fibroblasts reorient directionality by a metastable, PI3K-dependent mechanism

Erik S. Welf, Shoeb Ahmed, Heath E. Johnson, Adam T. Melvin, and Jason M. Haugh

Department of Chemical and Biomolecular Engineering, North Carolina State University, Raleigh, NC 27695

Mesenchymal cell migration as exhibited by fibroblasts is distinct from amoeboid cell migration and is characterized by dynamic competition among multiple protrusions, which determines directional persistence and responses to spatial cues. Localization of phosphoinositide 3-kinase (PI3K) signaling is thought to play a broadly important role in cell motility, yet the context-dependent functions of this pathway have not been adequately elucidated. By mapping the spatiotemporal dynamics of cell protrusion/retraction and PI3K signaling monitored by total internal reflection fluorescence microscopy, we show that randomly migrating fibroblasts reorient polarity through PI3K-dependent branching and pivoting of protrusions. PI3K inhibition did not affect the initiation of newly branched protrusions, nor did it prevent protrusion induced by photoactivation of Rac. Rather, PI3K signaling increased after, not before, the onset of local protrusion and was required for the lateral spreading and stabilization of nascent branches. During chemotaxis, the branch experiencing the higher chemoattractant concentration was favored, and, thus, the cell reoriented so as to align with the external gradient.

Introduction

Control of cell crawling behavior is fundamental to collective and concerted movements of multiple cell types, as seen during embryonic development and physiological responses to wounding and infection. To achieve productive migration, a cell must be spatially polarized, with differential localization of signaling, adhesion, and cytoskeletal processes to promote net protrusion at one end and net retraction at the other (Ridley et al., 2003). Maintenance of this fore-aft asymmetry is the basis for directional persistence, whereby a randomly migrating cell moves along fairly straight paths for sustained periods, punctuated by stochastic turning behavior that causes changes in orientation (Petrie et al., 2009). It follows that regulation of cell turning determines the fidelity of cell migration directed by chemotactic gradients and other dynamic and potentially competing spatial cues. Changes in direction should be suppressed while the chemotaxing cell is properly aligned with the gradient; otherwise, cell turning ought to be encouraged and biased so as to steer the cell in the proper direction.

During the past decade, directed cell migration has been characterized in two distinct ways that are, separately, best understood in the context of the chemotactic amoeba *Dictyostelium discoideum*. One line of investigation concerns the polarization of intracellular signaling activities. Steep external gradients of cAMP elicit robust symmetry breaking, with Ras and phosphoinositide 3-kinase (PI3K) signaling localized with F-actin at the leading edge, in *D. discoideum* (Merlot and Firtel, 2003; Van Haastert and Devreotes, 2004); characteristic of amoeboid cells, actin polymerization is balanced by squeezing forces mediated by myosin localized at the cell rear. Whereas early studies implicated polarization of PI3K signaling in gradient sensing, it is now appreciated that its role is context dependent and that PI3K mediates only one of a few pathways known to be important for *D. discoideum* chemotaxis (Loovers et al., 2006; Hoeller and Kay, 2007; Takeda et al., 2007; Bosgraaf et al., 2008; Swaney et al., 2010). In the absence of a spatial cue, these pathways spontaneously polarize to govern random *D. discoideum* motility (Postma et al., 2003; Sasaki et al., 2007).

The other approach has been to characterize the morphological dynamics associated with leading-edge protrusion. *D. discoideum* cells crawl by extending morphologically defined protrusions (pseudopods). Chemotaxing amoebae extend pseudopods with a characteristic frequency, with new pseudopods primarily branching from existing ones (Andrew and Insall, 2007). Directional persistence is maintained by extending

The Rockefeller University Press $30.00
J. Cell Biol. Vol. 197 No. 1   105–114
www.jcb.org/cgi/doi/10.1083/jcb.201108152

JCB   **105**

pseudopods in an ordered manner, alternating between left and right of the cell migration axis (Bosgraaf and Van Haastert, 2009b). In the phenomenological model that has emerged, the cAMP gradient spatially biases an otherwise stochastic and excitable polarization process (van Haastert and Postma, 2007; Bosgraaf and Van Haastert, 2009a; Van Haastert, 2010; Xiong et al., 2010); however, even in this relatively well-characterized system, the connection between signaling and cell shape dynamics is presently unclear. cAMP stimulation elicits the formation of self-organizing domains in which PI3K signaling is locally enriched, and new pseudopods later emerge at those locations (Postma et al., 2003). In this context, however, inhibition of PI3K does not fundamentally alter pseudopod dynamics; it simply reduces the frequency of pseudopod generation (Andrew and Insall, 2007).

In contrast to cells that exhibit amoeboid movement, such as *D. discoideum* and leukocytes, fibroblasts and other mesenchymal cells are slow moving and crawl by balancing actin polymerization and integrin-mediated adhesion dynamics at their leading edges (Vicente-Manzanares et al., 2009; Friedl and Wolf, 2010). During random migration, these cells often exhibit multiple competing protrusions (lamellipodia) radiating in different directions, which has been linked to their migration behavior (Petrie et al., 2009). Fibroblasts with reduced expression of the Rho family GTPase Rac1 are more elongated and move with greater directional persistence (Pankov et al., 2005) because cell protrusion and retraction are predominantly oriented along the migration axis. In another study, fibroblasts with muted expression of Rac1, Cdc42, and RhoG exhibited a similarly elongated morphology and a severe cell speed defect, but they oriented normally in a chemotactic (PDGF) gradient (Monypenny et al., 2009). On the time scale of seconds to minutes, the leading edge exhibits complex motility dynamics, including periodic protrusion/retraction switching (Abercrombie et al., 1970; Giannone et al., 2004) and lateral protrusion waves (Döbereiner et al., 2006; Machacek and Danuser, 2006; Weiner et al., 2007). Through the combined use of fluorescent biosensors and high-resolution image analysis, the spatiotemporal relationships between activation of Rho family GTPases and such leading-edge morphodynamics have been elucidated (Sabouri-Ghomi et al., 2008; Machacek et al., 2009); however, given that the directionality of fibroblast migration is relatively long lived, with estimated persistence times in the range of 20–70 min (Gail and Boone, 1970; Dunn and Brown, 1987; Ware et al., 1998), it is presently unclear how overall cell shape changes associated with reorientation/turning behaviors are coordinated at the level of intracellular signaling.

Here, spatiotemporal mapping of protrusion/retraction, PI3K signaling, and morphological dynamics in fibroblasts reveals that although membrane protrusion and recruitment of PI3K signaling are relatively short lived, directional persistence is maintained by restricting where protrusion occurs. To achieve large-scale turns, migrating fibroblasts reorient migration polarity through branching and pivoting of lamellipodia. Inhibition of PI3K signaling blocks fibroblast reorientation by this mechanism, not by reducing the frequency of initiating new branches but rather their stability. Accordingly, localized PI3K signaling

increases after, not before, the initiation of protrusion induced spontaneously or by liberation of photoactivatable Rac. Finally, it is shown that biasing the branch-and-pivot reorientation mechanism allows chemotactic fibroblasts to align migration directionality with the external gradient. We conclude that, unlike *D. discoideum* responding to cAMP, lamellipodial branching in fibroblasts is not a regular mechanism of motility but rather a stochastic process that resets migration polarity. The critical role of PI3K signaling in this process is not in the generation of new protrusions but rather in promoting lateral spreading and propagation of the branched state.

Results

Reorientation of cell migration by coordination of motility dynamics across disparate time scales

We previously showed that PI3K signaling, monitored by total internal reflection fluorescence (TIRF) microscopy in migrating fibroblasts expressing the GFP-AktPH biosensor, is localized in protrusive structures during both random migration (Weiger et al., 2009, 2010) and chemotaxis (Melvin et al., 2011), and, thus, the pattern of PI3K signaling correlates with overall direction of cell migration (Fig. 1 a and Video 1). Furthermore, PI3K signaling is transient, with localized regions (hotspots) emerging and dying out, with a characteristic time scale of ~15 min in randomly migrating cells; the dynamics are globally coupled, in the sense that the emergence of a hotspot tends to be shortly followed or preceded by the death of another (Weiger et al., 2010).

Here, for the same cohort of randomly migrating cells ($n = 28$), we mapped the radial protrusion/retraction velocity alongside the locations of PI3K-signaling hotspots and regions of fingerlike morphological extension as a function of angular position (relative to the cell centroid) and time (Fig. 1 b). These spatiotemporal maps reveal distinct dynamics on short and long time scales (minutes vs. hours). Whereas individual protrusion and signaling events tend to be relatively short lived, consistent with the previous analysis (Weiger et al., 2010), they are almost exclusively confined to long-lived morphological extensions of the cell. Thus, protrusion and retraction occur along well-defined tracks in the spatiotemporal map (Fig. 1 b). Accordingly, across the cell population, PI3K signaling and protrusion are positively correlated, but the correlation of morphological extension with either protrusion or signaling is even greater (Fig. S1).

The dynamics of protrusion and retraction determine changes in cell shape and directionality. Whereas persistent protrusion at one end of a cell combined with retraction at the other end results in a smooth and straight migration path, deviation from that behavior causes cell reorientation. As illustrated in Fig. 1 (a and b), cells execute dramatic turns by pivoting of protruding structures, characterized by a change in angular position with time, most often preceded by branching of a protrusion into two. Thus, if the two branches continue to extend symmetrically, the cell can achieve a turn of up to 90°. This appears to be a generic behavior exhibited by cells of mesenchymal origin; examples are found in time-lapse videos accompanying recent
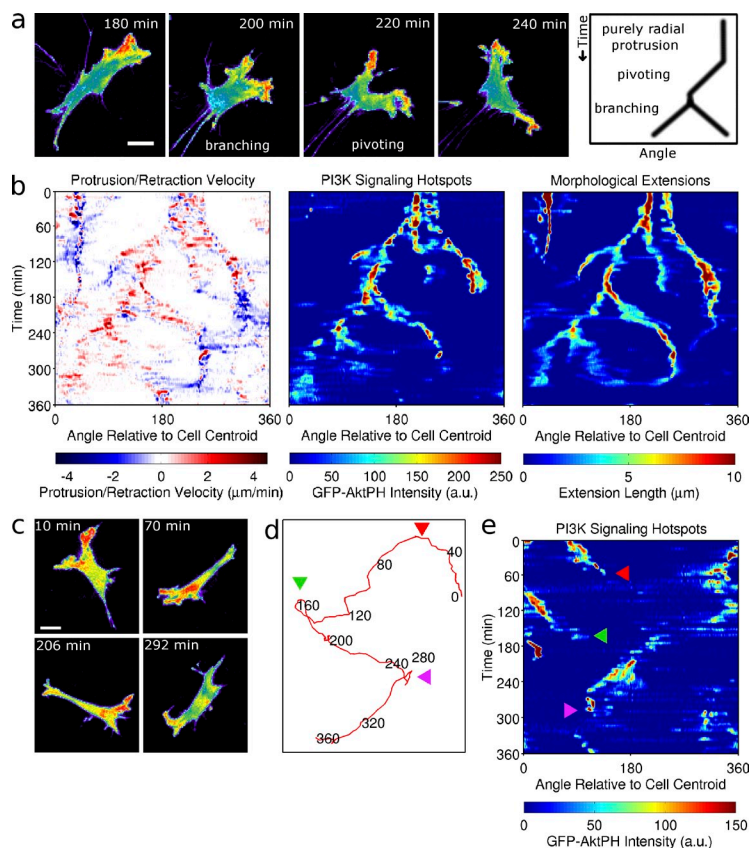
Figure 1. **Reorientation of fibroblast migration by branch and pivot of protrusions.** NIH 3T3 fibroblasts expressing GFP-AktPH were monitored by TIRF microscopy during random migration on fibronectin (n = 28). (a) A pseudocolor montage showing the characteristic branching and pivoting of protrusions and localization of PI3K signaling (see also Video 1). The sketch at the right illustrates how protrusion velocity, mapped as a function of angular position and time, reveals branch-and-pivot behavior. Bar, 20 µm. (b) Spatiotemporal maps of protrusion (red)/retraction (blue) velocity, PI3K-signaling hotspots, and morphological extensions for the cell depicted in a. a.u., arbitrary unit. (c–e) Protrusion branching and switching between protrusion and retraction mediate sharp turns. A pseudocolor montage (c; see also Video 2), contact area centroid path (d), and spatiotemporal map of PI3K-signaling hotspots (e) show how abrupt changes in cell orientation correspond with changes in PI3K signaling (colored arrowheads). Bar, 20 µm.

publications (Lo et al., 2004; Pankov et al., 2005; Monypenny et al., 2009; Uetrecht and Bear, 2009). Another characteristic behavior is switching of a region between net protrusion, which is accompanied by intermittent PI3K signaling, and net retraction, during which PI3K signaling is silent. This behavior allows the cell to effectively reverse polarity and thus execute sharper changes in direction (Fig. 1 [c–e] and Video 2).

PI3K signaling promotes cell reorientation through dilation and stabilization of newly branched lamellipodia

The preceding analysis suggests that the stochastic dynamics of PI3K signaling and protrusion are coupled to the longer–time scale dynamics associated with cell turning. If so, interfering with PI3K signaling would be expected to alter turning behavior. Using a potent pharmacological inhibitor with selectivity for type IA PI3Ks (PI3K-α inhibitor IV), titrated to a concentration (500 nM) that was just sufficient to almost fully inhibit PI3K signaling in most cells, we compared cell motility before and after addition of the drug (Fig. 2 a and Video 3). Strikingly, PI3K-inhibited cells adopt a more elongated morphology, with protrusion restricted to the poles. Although short-lived bifurcations were sometimes noticeable in the spatiotemporal protrusion map, stable branching and pivoting were virtually absent. The specificity of this effect was corroborated using a dominant-negative mutant of PI3K regulatory subunit p85-α (Dhand et al., 1994); cells expressing this construct exhibited the same crawling phenotype as the drug-treated cells (Fig. 2 b and Video 4).

To examine the morphodynamics of branched protrusions in greater detail, we monitored fibroblasts coexpressing GFP-AktPH and tdTomato-Lifeact, a marker of F-actin, during random migration; during the course of such experiments, PI3K-α inhibitor IV was sometimes added (Fig. 2 c and Video 5). Without PI3K inhibited, newly formed branches consistently become enriched in PI3K signaling and spread laterally (dilate) as they protrude, with a band of F-actin that broadens along the leading edge. Analysis of AktPH and Lifeact accumulation shows that these processes temporally overlap (Fig. 2 d). With PI3K inhibited, nascent protrusions still form with regularity, but they fail to broaden and stabilize, and they almost invariably stall and eventually retract (Fig. 2 c). Inspection of cells expressing the dominant-negative PI3K regulatory subunit confirmed that nascent protrusions fail to dilate and are unstable when PI3K cannot be recruited (Fig. 2 e).

Quantitative analysis revealed that inhibition of PI3K by either approach does not grossly affect the overall frequency of initiated branches, defined as the emergence of a protrusion in a distinct direction. Rather, PI3K inhibition prevents successful propagation of the branched state (Fig. 2 f). To evaluate how the inability to branch and pivot impacts overall cell migration, motility metrics of control and dominant-negative p85-expressing cells were compared (Fig. 2 g). PI3K inhibition did not significantly affect the overall migration speed or directional persistence (D/T ratio) of the cell population, whereas the PI3K-inhibited cohort showed reduced rates of protruded area generation and less sideways movement, as judged by the ratio of elliptical axes of each cell's migration path (Fig. 2 g).

Figure 2. PI3K signaling is required for propagation but not initiation of branched protrusions. (a) Protrusion/retraction map and pseudocolor TIRF images of a randomly migrating fibroblast expressing GFP-AktPH; PI3K-α inhibitor IV (500 nM) was added at approximately the midway point (see also Video 3). Red arrowheads in the image mark sites of protrusion/retraction. The results are representative of 12 cells. Bar, 20 µm. (b) Protrusion/retraction map and pseudocolor TIRF image of a randomly migrating fibroblast coexpressing the dominant-negative PI3K regulatory subunit and GFP-AktPH (see also Video 4). The results are representative of nine cells. Bar, 20 µm. (c) TIRF montage of a randomly migrating fibroblast expressing GFP-AktPH and tdTomato-Lifeact; PI3K-α inhibitor IV (500 nM) was added after ∼3 h (see also Video 5). Arrowheads mark sites of protrusion with F-actin at the leading edge. The results are representative of 10 cells. Bar, 10 µm. (d) A linescan showing temporal overlap of AktPH and Lifeact accumulation in a transient protrusion. The TIRF images at the right show the position of the linescan and correspond to the time indicated by arrowheads on the left. Bar, 10 µm. (e) Nascent protrusions (arrowheads) are thin and short lived in cells coexpressing the dominant-negative PI3K regulatory subunit and GFP-AktPH. Bar, 10 µm. (f) Quantification of branch initiation and successful branch propagation (total number of events divided by total time) with versus without PI3K inhibition (Inhib.). The

control cells (n = 28) are the same as analyzed in Fig. 1, DN p85 refers to cells expressing the dominant-negative PI3K regulatory subunit (n = 9), and the other cohorts are cells before and after treatment with PI3K-α inhibitor IV (n = 12). (g) Cell motility metrics comparing the control and DN p85 cohorts as described in f. Mean cell centroid translocation speed, D/T ratio (direct distance from start to end divided by the total distance traveled), and mean protruded area generation were evaluated for 12-min intervals. The cell path axis ratio measures each cell's degree of sideways movement relative to the major axis of migration.
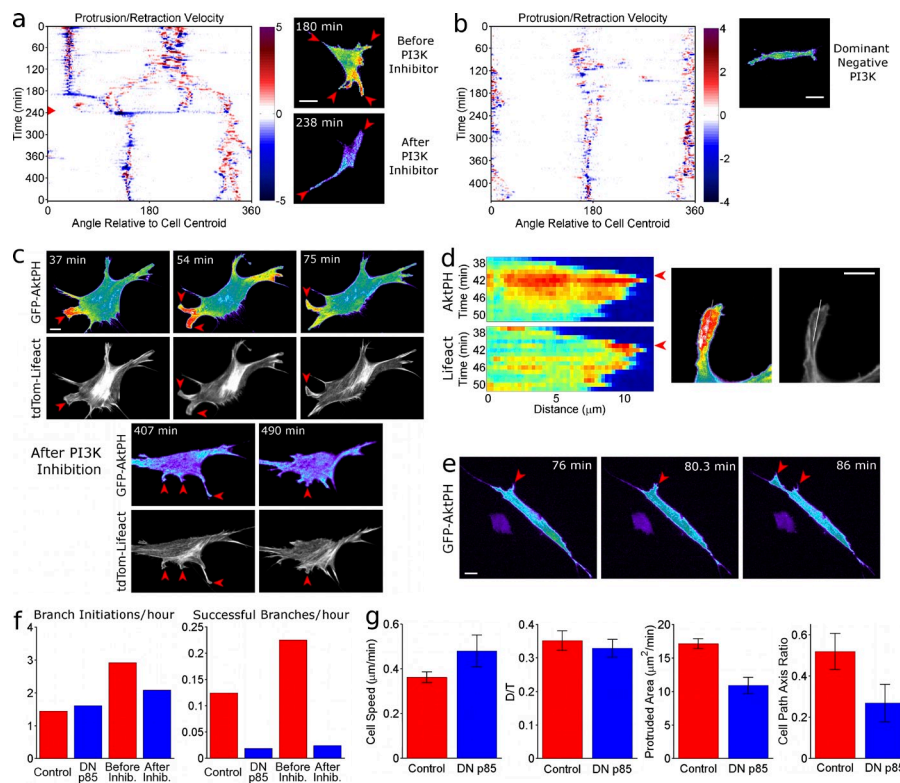
The lack of effect on directional persistence was unexpected; retrospective analysis of the cell centroid tracks indicated that the PI3K-inhibited cells' movements showed more back-and-forth reversals of direction that nonetheless lay along a nearly parallel path. Collectively, these results demonstrate that PI3K signaling, rather than serving as a prerequisite for protrusion by itself, reinforces newly formed lamellipodia to promote large-scale turns in cell migration.
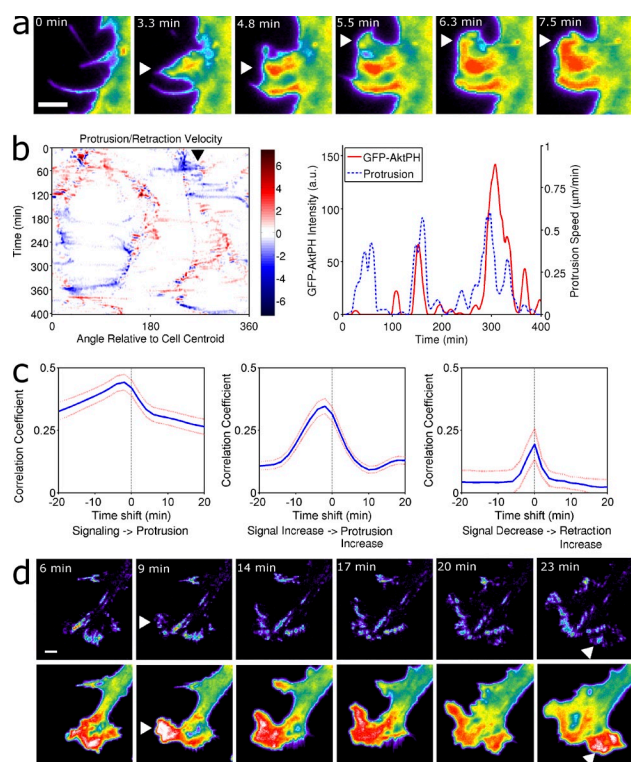
PI3K signaling is localized after initiation of protrusion

To better define the relationship between local activation of PI3K signaling and leading-edge protrusion, we sought to determine the temporal sequence of these two processes. Somewhat surprisingly, inspection of time-lapse images (Fig. 3 a) and time series taken at fixed angular positions (Fig. 3 b) revealed that localization of PI3K signaling tends to lag the onset of protrusion. Dual TIRF imaging of cells coexpressing mCherry-AktPH and teal fluorescent protein confirmed that regions of AktPH accumulation are reasonably uniform in their apposition with the surface and that they do not introduce an artifact in locating the edge position (Fig. S2). Correlation of protrusion velocity and PI3K hotspot fluorescence with variable time lag (for all angular positions and cells) peaks with protrusion preceding signaling by ∼1–2 min (Fig. 3 c); the peak is sharpened considerably by correlating the positive derivatives

(changes with respect to time) of the measurements, indicating that PI3K signaling increases in intensity after the movement of the leading edge begins to accelerate. Whereas PI3K signaling increases after initiation of protrusion, the reverse process—loss of PI3K signaling accompanied by net retraction—occurs with no perceptible time lag (Fig. 3 c). Dual TIRF imaging of cells coexpressing mCherry-AktPH and GFP-paxillin, a marker of integrin-mediated adhesions (Laukaitis et al., 2001), shows that PI3K signaling increases during the transition of the adhesions from nascent to mature (Fig. 3 d and Video 6), underscoring the spatiotemporal coordination of signaling and adhesion dynamics in lamellipodia.
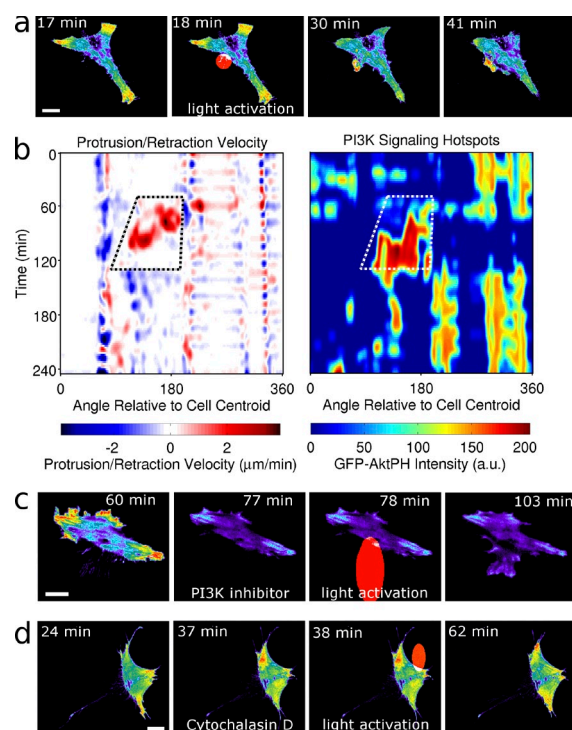
Protrusion induced by focally activated Rac is followed by redistribution of PI3K signaling

The results presented thus far suggest that PI3K signaling is not required for leading-edge protrusion or maintenance of overall cell migration speed; rather, PI3K signaling is mobilized after protrusion and subsequently promotes lateral spreading and propagation of the branched state. To further test this hypothesis, we used a fusion protein construct (PA-Rac) that enables reversible photoactivation of Rac signaling; by focusing blue-green light in a particular region of the cell, one can control the timing and location of Rac-induced protrusion (Wu et al., 2009). Indeed, focal activation of PA-Rac in cells coexpressing

Figure 3. **PI3K signaling is localized after initiation of protrusion.** (a) A pseudocolor montage illustrating local membrane protrusion followed by increases in GFP-AktPH localization in a randomly migrating fibroblast. White arrowheads indicate local protrusion events and ensuing increases in PI3K signaling. Bar, 5 µm. (b) Protrusion/retraction map for a representative cell migration experiment alongside a plot showing the time courses of positive protrusion velocity and PI3K signaling localization at the angular position marked by the black arrowhead. (c) Time-lagged correlations of PI3K signaling localization with positive protrusion velocity (left) and of their positive time derivatives (increase in signaling with increase in protrusion; middle) and of the negative time derivative of PI3K signaling localization with the negative derivative of retraction velocity (increase in retraction; right) for the cohort of randomly migrating fibroblasts. Correlation coefficients were calculated for each cell, and the aggregate values are reported as mean ± 95% confidence interval ($n = 28$). (d) Fibroblasts coexpressing mCherry-AktPH (top) and GFP-paxillin (bottom) were monitored by TIRF microscopy during random migration (see also Video 6). White arrowheads indicate local increases in PI3K signaling coinciding with transition of adhesions from nascent to mature. Bar, 5 µm.

mCherry-AktPH catalyzed local protrusion from the sides of the cells (Fig. 4 a and Video 7). After initiation of protrusion, a clearly defined PI3K hotspot was formed at the site of photoactivation in 95% of the cells tested ($n = 42$); often, the hotspot emerged in tandem with reduction or disappearance of enriched PI3K signaling elsewhere (Fig. 4 b), as expected based on the dynamic coupling of hotspots previously described (Weiger et al., 2010). Consistent with the results presented in Fig. 2, PA-Rac–induced protrusion was equally robust in PI3K-inhibited cells (Fig. 4 c and Video 8). Finally, in support of the hypothesis that PI3K hotspot formation is associated with protrusion and not a byproduct of supraphysiological Rac signaling, PA-Rac failed to induce protrusion and hence did not dramatically alter the PI3K signaling pattern in cells with actin polymerization inhibited by addition of 200 nM cytochalasin D (Fig. 4 d and Video 9). Other experiments using cytochalasin D (Fig. S3) further support the notion that

Figure 4. **PI3K signaling is localized in response to protrusion induced by focally activated Rac.** (a) Localization of mCherry-AktPH in fibroblasts coexpressing PA-Rac was monitored by TIRF microscopy, as shown in the pseudocolor montage. Photoactivation of PA-Rac was initiated at the 18-min mark in the region indicated by the red oval and was maintained there until after the 41-min image shown (see also Video 7). Bar, 20 µm. (b) For another cell, spatiotemporal maps of protrusion/retraction velocity and PI3K signaling localization show the typical patterns before, during (indicated by the dashed polygons), and after PA-Rac photoactivation. The results are representative of 42 cells. a.u., arbitrary unit. (c) PA-Rac still elicits protrusion in cells treated with 1 µM PI3K-α inhibitor IV (see also Video 8). The results are representative of six cells treated with 0.5, 1, or 3 µM inhibitor. Bar, 20 µm. (d) Blocking protrusion by treatment with 200 nM cytochalasin D before photoactivation of PA-Rac prevents dramatic relocalization of PI3K signaling (see also Video 9). The results are representative of 11 cells thus treated. Bar, 20 µm.

protrusion directs the dynamic redistribution of PI3K signaling but is not required for maintenance of PI3K hotspots in morphological extensions.

Branch-and-pivot steering allows cells to align with a chemotactic gradient

We have shown that PI3K-dependent branching and pivoting of protrusions mediates fibroblast turning behavior and thus governs directional persistence of random migration. Fibroblast migration is directed by chemotactic gradients of PDGF, as during the proliferative phase of wound healing, and, therefore, we reasoned that cell turning would be important for the cell to become better oriented in the direction of the external gradient and to adjust to transient or competing spatial cues. Under optimal gradient conditions, PDGF elicits robust polarization of PI3K signaling (Schneider and Haugh, 2005), and the pattern of PI3K hotspot localization is quantitatively correlated with the fidelity of PDGF-stimulated chemotaxis (Melvin et al., 2011).

We observed chemotaxis of GFP-AktPH–expressing fibroblasts in the presence of PDGF-loaded alginate microspheres.

By this method, steep chemotactic gradients are achieved, and one can find various arrangements of chemoattractant sources (Melvin et al., 2011). When faced with a choice between two PDGF sources of similar strength, we observe that fibroblasts are sometimes attracted toward both; frequently, the cells choose one or the other, but, in this case, the steepest PDGF gradient lies between the two sources (Fig. 5 a and Video 10). To execute the ~90° turn that is required, one end of the cell branches and pivots and maintains strong PI3K signaling in the branch that ultimately aligns toward the sharpest gradient (Fig. 5 b). The other branch pivots around to the rear and later retracts. In the cohort of chemotaxing cells observed, a total of 30 successful branches were identified and scored according to whether or not one of the branches exhibited markedly higher protrusion velocity or PI3K signaling. The most common outcome, seen 40% of the time, was for both protrusion and signaling to be greater in the branch that became better aligned with the PDGF gradient (Fig. 5 c). Most often, lamellipodial pivoting resulted in improved alignment of migration directionality, as judged by the change in cell movement angle relative to the gradient (Fig. 5 d).

In a separate set of experiments, we challenged GFP-AktPH–expressing cells with a PDGF gradient, introduced by flow from a micropipette, oriented such that the gradient was initially oriented at roughly a 90° angle relative to the cell's long axis. In these experiments, when the cell properly reoriented toward the gradient (which was observed in six of eight motile cells), it invariably did so by successful propagation of the branched state (Fig. 5 e). In this experimental context, we also tested cells in which recruitment of PI3K was inhibited by co-expression of dominant-negative p85. In these cells, reorientation was achieved less frequently (in four of nine motile cells); more often, these cells continued to move perpendicular to the gradient (Fig. 5 e). In those instances when the dominant-negative p85-expressing cells reoriented, hotspots of PI3K signaling were observed in the branched protrusions. This suggests that PDGF gradient stimulation induced local recruitment of PI3K (overcoming the antagonism of the dominant negative) or/and local reduction of 3′ phosphoinositide dephosphorylation; evidence for the latter effect in PDGF-stimulated fibroblasts has been reported (Schneider et al., 2005). Collectively, our results indicate that branch-and-pivot shape changes are initiated stochastically to affect fibroblast reorientation and that chemotactic gradients bias this process to align cell movement toward an attractant source.

Discussion

A conceptual model of branch-and-pivot turning

Based on our observations and analyses, we propose the following scheme for fibroblast reorientation (Fig. 6). First, a lamellipodium develops a newly initiated branch. This occurs stochastically but with reasonable frequency (once or twice per hour) and is PI3K independent. In tandem with the newly formed protrusion, PI3K is recruited, and its lipid products accumulate with a characteristic time scale of ~1 min (Schneider and Haugh, 2004). PI3K signaling is required for dilation and stabilization of the branched state; in its absence, the nascent
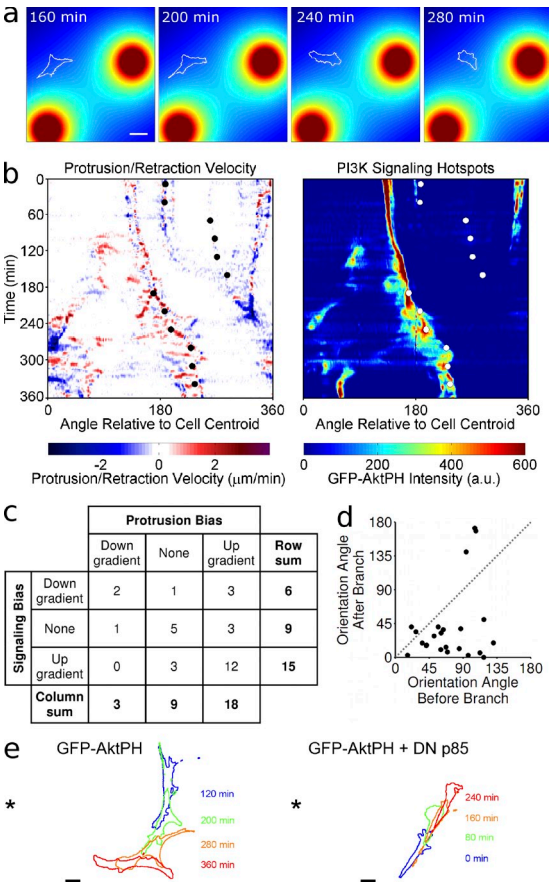
Figure 5. **Fibroblast reorientation is biased by a PDGF gradient.** (a–d) GFP-AktPH–expressing cells were monitored by TIRF microscopy during migration in the presence of alginate microspheres loaded with PDGF. (a) A pseudocolor montage indicating the calculated PDGF concentration field and outline of a chemotactic cell (see also Video 10). Bar, 50 µm. (b) Spatiotemporal maps of protrusion/retraction velocity and PI3K signaling localization for the cell depicted in a. The angular position of maximum PDGF concentration as a function of time is indicated by circle symbols to show the alignment of the cell with the external gradient. The results are representative of 25 cells that exhibited reorientation behavior. a.u., arbitrary unit. (c). A total of 30 branching events in the chemotaxing cells was scored according to whether they exhibited biases (markedly more in one branch than the other) in protrusion velocity and/or PI3K signaling localization and, if so, whether the dominant branch experienced the higher or lower PDGF concentration. (d) When the absolute angles of cell movement relative to the gradient (0–180°, with 0° corresponding to perfect alignment) before and after a successful branching event could be clearly determined, these angles were compared by scatter plot. Points below the $y = x$ (dotted) line represent branching events that resulted in improved alignment. (e) Overlaid outlines of GFP-AktPH–expressing fibroblasts, each responding to a PDGF gradient introduced by a micropipette (position indicated by an asterisk) oriented roughly perpendicular to the cell's long axis. The cell on the right shows the more characteristic behavior of cells coexpressing the dominant-negative PI3K regulatory subunit. Times after initiation of the gradient are indicated. Bars, 20 µm.

protrusion stalls and eventually retracts. Even after dilating successfully, reorientation is most often unsuccessful. This, we speculate, is linked to the inherently dynamic pattern of PI3K localization, in which distant regions of PI3K signaling globally compete with one another (Weiger et al., 2010). To the extent that PI3K signaling can be maintained, the branched state propagates. We consider this process to be metastable, as it is self-limiting; taken to its fullest extent, the two branches end up at opposite ends of the cell, and the cell executes a near-90° turn.
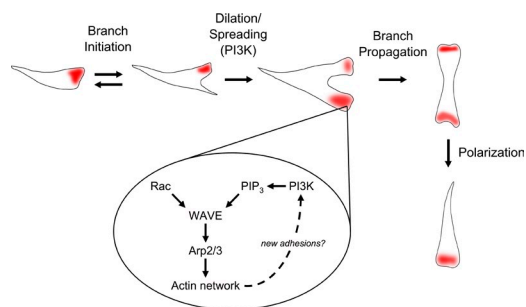
Figure 6. **Conceptual model of fibroblast reorientation by branch-and-pivot dynamics.** Cells with a defined front and rear at opposite ends are considered stable, and deviations from this morphology are unstable. Nascent branches are initiated stochastically and in a PI3K-independent manner. After the onset of protrusion, PI3K is localized there; PI3K signaling is required for lateral spreading and stabilization of the new lamellipodium. If PI3K signaling is not interrupted (for too long) in either of the two branches, the branched state is metastable and propagates. A turn of up to 90° is completed once one of the branches stops protruding and reverts to net retraction. The inset outlines a hypothetical feedback loop in which protrusion and PI3K signaling reinforce one another.

The process is resolved once one of the ends switches from net protrusion to net retraction, at which point the cell is stably polarized and reoriented.

On the emergence and stabilization of protrusion branching

The spatiotemporal protrusion maps (as in Fig. 1) show that protrusion and retraction are limited to a few extended structures of the cell, providing the basis for fibroblasts' directional persistence. Protrusion rarely occurs along the cell sides, where mature actomyosin stress fibers are under contractile tension (although liberation of PA-Rac can apparently overcome this barrier after a delay). Within the permissive regions, protrusions emerge as discrete bursts, seen as punctate spots on the spatiotemporal maps. The branched structure is favored because new protrusion bursts are forced to emerge in the vicinity of previous ones.

The localized nature of productive protrusion is consistent with the overlapping dynamics associated with the lamellar versus lamellipodial actin networks characterized in epithelial cells (Ponti et al., 2004; Danuser, 2005). The dendritic lamellipodial network is not required for protrusion per se; rather, through the actions of Arp2/3 and cofilin, it appears to maintain and broaden the leading edge after a localized protrusion event (Gupton et al., 2005). Such a mechanism implies a role for PI3K signaling, which alongside Rac promotes Arp2/3 function at the leading edge by activating WAVE complexes (Fig. 6, inset; Oikawa et al., 2004; Sossey-Alaoui et al., 2005; Lebensohn and Kirschner, 2009). Two observations are consistent with this idea. First, fibroblasts with PI3K inhibited adopt an elongated morphology, with a narrow leading edge but no gross defect in cell speed, similar to those with Rac depleted (Pankov et al., 2005). Second, our results establish that PI3K signaling, like Rac and Cdc42 activation (Tsukada et al., 2008; Machacek et al., 2009), lags the onset of protrusion.

The mechanism outlined above explains how bifurcation of a protrusion might arise, but it does not address the metastability and propagation of the branched state. In that regard, we speculate

that myosin-driven maturation of adhesions and stress fibers (Vicente-Manzanares et al., 2007; Cirit et al., 2010) plays a critical role in stabilizing the cleft.

On the dynamic coordination of protrusion and PI3K signaling

Our spatiotemporal mapping analysis and PA-Rac experiments suggest that PI3K signaling responds to leading-edge protrusion. This could be mediated by, for example, newly formed nascent adhesions or through positive feedback associated with WAVE activation (Sossey-Alaoui et al., 2005; Millius et al., 2009). When protrusion was blocked by cytochalasin D treatment, we observed that PI3K signaling persists but is less dynamic. Therefore, just as PI3K is not required for protrusion but affects its character, protrusion is not required for maintenance of the overall PI3K signaling level but affects its dynamic redistribution under global competition. This passive form of positive feedback is consistent with the reported response to local release of dominant-negative Rac: rather than simply inhibiting protrusion in that region, protrusion was induced in distal regions of the cell (Wu et al., 2009).

These conclusions differ somewhat from those of Yoo et al. (2010), who studied the localization and function of PI3K signaling in migrating neutrophils imaged in live zebrafish. As in our system, PA-Rac induced protrusion and localization of PI3K signaling in these cells; however, PA-Rac did not elicit migration in neutrophils treated with PI3K inhibitors. This discrepancy might be attributed to differences in cellular/microenvironmental context.

On the control of gradient sensing and chemotaxis

In their analysis of *D. discoideum* motility, Andrew and Insall (2007) noted that protrusion branching is prominent in a variety of cell types, including fibroblasts. Our analysis reveals a mode of chemotaxis in fibroblasts that is, on the surface, reminiscent of *D. discoideum* motility, in the sense that one of the two branches is favored based on the orientation of the chemoattractant gradient. Just as the mechanics of amoeboid and mesenchymal migration are quite different, so too are the features of the branching phenomena in the two cell types. At least under certain conditions, *D. discoideum* cells branch pseudopods at a regular frequency to execute both modest turns or, through ordered branching, persistent migration (Andrew and Insall, 2007; Bosgraaf and Van Haastert, 2009a,b). In contrast, protrusion branching in fibroblasts occurs stochastically and, if propagated to the bipolar state, yields turns of up to 90°; persistent fibroblast migration is achieved when branching does not occur. In addition to the functional differences, the timing and role of PI3K signaling localization are also distinct. In *D. discoideum*, it has been reported that PI3K signaling patches coalesce before pseudopod formation (Postma et al., 2003), and PI3K inhibition reduces the frequency of pseudopod generation (Andrew and Insall, 2007). In fibroblasts, we have shown that PI3K signaling is localized after the onset of protrusion, and, accordingly, PI3K inhibition does not affect the initiation of branches but rather their ability to propagate.

The branch-and-pivot mechanism mediates large-scale reorientation of chemotaxing cells and, to the extent that the branches are chemoattractant-sensing elements, would aid in gradient perception by extending the branches apart from another. This is not to say that branching is required for gradient sensing or chemotaxis, especially in cells with much broader lamellipodia. On the contrary, once fibroblasts are polarized and migrating with only modest deviations from the gradient axis, they track the gradient by making only small turns associated with subtle morphology changes (Arrieumerlou and Meyer, 2005; Melvin et al., 2011).

Materials and methods

Cell culture, DNA constructs, and other reagents
NIH 3T3 cells (American Type Culture Collection) were cultured, and stable expression of GFP- or mCherry-AktPH was achieved by retroviral infection and puromycin selection, as previously described (Weiger et al., 2009). The mCherry-AktPH-pBM-IRES-Puro retroviral vector was constructed by cloning mCherry into the same position as EGFP in the previously described EGFP-AktPH-pBM-IRES-Puro vector (Weiger et al., 2009), encoding the fusion of the fluorescent protein to the N terminus of the AktPH domain (residues 2–149 of murine Akt1). Transient coexpression of other constructs was achieved by lipofection. EGFP-AktPH-C1 and mCherry-AktPH-C1 are transient expression vectors that encode the same fusion proteins as their retroviral counterparts (Weiger et al., 2009). The dominant-negative p85-α vector encodes a mutant of bovine PI3K regulatory subunit p85-α with the p110 binding site deleted (p85-αΔ478-513; Dhand et al., 1994). The tdTomato-Lifeact plasmid, expressing a fusion of tdTomato and the Lifeact peptide (Riedl et al., 2008), was a gift from J. Bear (The University of North Carolina at Chapel Hill, Chapel Hill, NC). The GFP-paxillin vector, expressing a fusion of EGFP and full-length paxillin, was constructed in the laboratory of R. Horwitz (University of Virginia, Charlottesville, VA; Addgene plasmid 15233; Laukaitis et al., 2001). The vector encoding the fusion of mCerulean and PA-Rac (N-term2) was a gift from Y. Wu and K. Hahn (The University of North Carolina at Chapel Hill, Chapel Hill, NC). Human plasma fibronectin was obtained from BD and Invitrogen. PI3K-α inhibitor IV was purchased from EMD, and cytochalasin D was purchased from Sigma-Aldrich.

Cell migration experiments
Glass coverslips were cleaned, sterilized, coated with 10 µg/ml fibronectin (BD) for 1 h at 37°C, washed with deionized sterile water, and dried within 30 min of the experiment. Cells were detached with a brief trypsin-EDTA treatment and suspended in the imaging buffer (20 mM Hepes, pH 7.4, 125 mM NaCl, 5 mM KCl, 1.5 mM MgCl$_2$, 1.5 mM CaCl$_2$, 10 mM glucose, 1% vol/vol FBS, and 2 mg/ml fatty acid–free BSA). After centrifugation at 100 g for 3 min, the cells were resuspended in imaging buffer and plated on the fibronectin-coated coverslips at a density of ∼10,000 cells/ml and allowed to spread for 1–2 h before imaging. Mineral oil was layered on top of the buffer to prevent evaporation. Chemotaxis experiments using alginate microspheres (a gift from D. Irvine, Massachusetts Institute of Technology, Cambridge, MA) were performed as previously described in detail (Melvin et al., 2011). In brief, sodium alginate microspheres were incubated in a solution of 1 µM PDGF-BB (25 µl) for 24 h at 4°C. Before imaging, the microspheres were washed and added to the cells. In other experiments as indicated, PDGF gradients were produced using a micropipette, pulled to a diameter of ∼30 µm, backfilled with a solution of 2 nM PDGF in imaging buffer, and controlled using a syringe pump (World Precision Instruments) and micromanipulator (Siskiyou, Inc.). All experiments were performed at 37°C.

Microscopy
Our prism-based TIRF microscope is a self-built rig built around an Axioskop 2 FS (Carl Zeiss; Schneider and Haugh, 2004). Excitation of EGFP (488 nm), mCherry (561 nm), tdTomato (561 nm), or teal fluorescent protein (442 nm) was achieved with an incident beam energy of roughly 20–50 mJ per image. Water dipping objectives (20×, 0.5 NA and 40×, 0.8 NA Achroplan; Carl Zeiss) were used along with a 0.63× camera mount. Digital images were acquired using a cooled charge-coupled device (ORCA ER; Hamamatsu Photonics) and MetaMorph software (Universal Imaging).

Photoactivation of PA-Rac was achieved using a 50-W mercury arc lamp passed through a 436/20-nm excitation filter. A focal pattern of light was created by focusing the lamp lens and blocking diffuse light in the light path. A fluorescent dextran solution was used to quantify the spatial profile of excitation, and a threshold was applied to define the region of photoactivation.

Image analysis
All image analysis was performed using MATLAB (MathWorks). The methods used for identification and spatiotemporal mapping of protruded/retracted areas, PI3K-signaling hotspots, and extended morphological structures are described below and illustrated in Fig. S4.

The protruded areas for each time interval are identified as pixels associated with the cell in the present image but not in the previous image and vice versa for the retracted areas. For each protruded or retracted pixel, the angle between the pixel and the cell centroid (relative to the negative x axis) was calculated and rounded to the nearest whole angle. Protrusion or retraction velocity was calculated as the net change in number of protruded/retracted pixels along the indicated angle (multiplied by the pixel size) divided by the change in time (Fig. S4 a). This approach is simple and unambiguous in its implementation, and we find it to be a robust method for image stacks with modest spatial and temporal resolution, as was the case here. More sophisticated protrusion mapping methods have been described (Machacek and Danuser, 2006; Bosgraaf et al., 2009).

Image segmentation to identify pixels associated with PI3K-signaling hotspots was performed as previously described in detail (Weiger et al., 2009, 2010). In brief, the k-means clustering method was used, with $k = 4$, and hotspots were identified as those regions with at least 20 contiguous pixels in the highest-intensity bin. Those pixels were mapped according to their angles relative to the cell centroid, with the value given in the heat map calculated as the sum of background-subtracted fluorescence intensities for all pixels that lie along the indicated angle (Fig. S4 b).

Extended morphological structures were identified as follows. Each fluorescence intensity image was thresholded, and the pixels defining the cell perimeter were indexed according to their relative positions. The local mean distance of the cell periphery from the cell centroid (averaged over 20 adjacent pixels) was calculated for each indexed location, and pixels that were >1 µm beyond the local mean were considered associated with extended morphological structures. These structures were smoothed by a standard morphological opening operation, and, finally, the contour of the region was enlarged (dilated) by 5 pixels on each side. Pixels associated with the structures thus identified were mapped according to their angles relative to the cell centroid, with the value given in the heat map calculated as the number of pixels lying along the indicated angle (Fig. S4 c).

For the purposes of graphical presentation and correlation analysis, the protrusion velocity, hotspot signaling, and morphological extension metrics were smoothed using a weighted linear least squares and a first-degree polynomial model using spatial and temporal spans of 5° and five frames, respectively. For the correlation of time derivatives, a span of 10° and 10 frames was used. Cross-correlations between the mapped protrusion, signaling, and morphology metrics, binned into 10-degree angle intervals, were calculated using the MATLAB function $normxcorr2$. To confirm that the correlations involving local protrusion are not influenced by potential artifacts associated with binning protruded pixels by angle relative to the centroid, the correlation calculations were repeated using a more selective protrusion-mapping method. In the modified algorithm, among the protruded or retracted pixels found in a particular angular bin, only those belonging to the contiguous region located furthest from the centroid were included (Fig. S4 d). We confirmed that the use of this approach did not affect any of our conclusions, including the temporal offset between protrusion and signaling (Fig. S4 e).

Cell motility metrics were calculated by manual thresholding of the TIRF images to identify the cell contact area. For each cell, cell speed was calculated as the mean of the instantaneous displacement of the contact area centroid sampled every 12 min. Migration path D/T was calculated by dividing the overall displacement of the cell centroid by the sum of the distances moved along the path of the centroid sampled every 12 min. The protruded area was calculated as the mean value of the instantaneous protruded area sampled every 12 min. The cell path axis ratio was calculated as the ratio of the minor and major axes of an ellipse having the same normalized second central moments as the cell path, which was determined by creating a pileup of the cell contact areas taken at 2-min intervals (Fig. S5).

Online supplemental material
Fig. S1 shows that PI3K signaling, membrane protrusion, and regions of morphological extension are spatiotemporally correlated during random

migration. Fig. S2 shows soluble teal fluorescent protein controls for detection of PI3K signaling in lamellipodia and of leading-edge protrusion. Fig. S3 shows that inhibition of actin polymerization during random migration does not disrupt PI3K signaling. Fig. S4 shows identification and spatiotemporal mapping of protruded/retracted areas, PI3K-signaling hotspots, and extended morphological structures. Fig. S5 shows the determination of cell path axis ratio. Video 1 shows a time-lapse TIRF video of a randomly migrating, GFP-AktPH–expressing cell, as depicted in Fig. 1 a. Video 2 shows a time-lapse TIRF video of a randomly migrating, GFP-AktPH–expressing cell, as depicted in Fig. 1 c. Video 3 shows a time-lapse TIRF video of a randomly migrating, GFP-AktPH–expressing cell, as depicted in Fig. 2 a; PI3K-α inhibitor IV (500 nM) was added midway through the experiment. Video 4 shows a time-lapse TIRF video of a randomly migrating cell coexpressing GFP-AktPH and the dominant-negative PI3K regulatory subunit, as depicted in Fig. 2 b. Video 5 shows parallel time-lapse TIRF videos of a cell coexpressing GFP-AktPH (top) and tdTomato-Lifeact (bottom), as depicted in Fig. 2 c; PI3K-α inhibitor IV (500 nM) was added at approximately the 3-h mark. Video 6 shows parallel time-lapse TIRF videos of a cell coexpressing GFP-paxillin (left) and mCherry-AktPH (right), as depicted in Fig. 3 d. Video 7 shows a time-lapse TIRF video of a randomly migrating cell coexpressing mCherry-AktPH and PA-Rac, as depicted in Fig. 4 a; the flashing spot indicates the time period and site of PA-Rac liberation. Video 8 shows a time-lapse TIRF video of a randomly migrating cell coexpressing mCherry-AktPH and PA-Rac, as depicted in Fig. 4 c; at the midway point, PI3K-α inhibitor IV (1 µM) was added, and the flashing spot shown thereafter indicates the time period and site of PA-Rac liberation. Video 9 shows a time-lapse TIRF video of a randomly migrating cell coexpressing mCherry-AktPH and PA-Rac, as depicted in Fig. 4 d. At the midway point, cytochalasin D (200 nM) was added, and the flashing spot shown thereafter indicates the time period and site of PA-Rac liberation. Video 10 shows a time-lapse TIRF video of a chemotactically migrating, GFP-AktPH–expressing cell presented in parallel with the calculated PDGF concentration field, as depicted in Fig. 5 a. Online supplemental material is available at http://www.jcb.org/cgi/content/full/jcb.201108152/DC1.

References

Abercrombie, M., J.E. Heaysman, and S.M. Pegrum. 1970. The locomotion of fibroblasts in culture. I. Movements of the leading edge. *Exp. Cell Res.* 59:393–398. http://dx.doi.org/10.1016/0014-4827(70)90646-4

Andrew, N., and R.H. Insall. 2007. Chemotaxis in shallow gradients is mediated independently of PtdIns 3-kinase by biased choices between random protrusions. *Nat. Cell Biol.* 9:193–200. http://dx.doi.org/10.1038/ncb1536

Arrieumerlou, C., and T. Meyer. 2005. A local coupling model and compass parameter for eukaryotic chemotaxis. *Dev. Cell.* 8:215–227. http://dx.doi.org/10.1016/j.devcel.2004.12.007

Bosgraaf, L., and P.J. Van Haastert. 2009a. Navigation of chemotactic cells by parallel signaling to pseudopod persistence and orientation. *PLoS ONE.* 4:e6842. http://dx.doi.org/10.1371/journal.pone.0006842

Bosgraaf, L., and P.J.M. Van Haastert. 2009b. The ordered extension of pseudopodia by amoeboid cells in the absence of external cues. *PLoS ONE.* 4:e5253. http://dx.doi.org/10.1371/journal.pone.0005253

Bosgraaf, L., I. Keizer-Gunnink, and P.J.M. Van Haastert. 2008. PI3-kinase signaling contributes to orientation in shallow gradients and enhances speed in steep chemoattractant gradients. *J. Cell Sci.* 121:3589–3597. http://dx.doi.org/10.1242/jcs.031781

Bosgraaf, L., P.J. van Haastert, and T. Bretschneider. 2009. Analysis of cell movement by simultaneous quantification of local membrane displacement and fluorescent intensities using Quimp2. *Cell Motil. Cytoskeleton.* 66:156–165. http://dx.doi.org/10.1002/cm.20338

Cirit, M., M. Krajcovic, C.K. Choi, E.S. Welf, A.F. Horwitz, and J.M. Haugh. 2010. Stochastic model of integrin-mediated signaling and adhesion dynamics at the leading edges of migrating cells. *PLOS Comput. Biol.* 6:e1000688. http://dx.doi.org/10.1371/journal.pcbi.1000688

Danuser, G. 2005. Coupling the dynamics of two actin networks—new views on the mechanics of cell protrusion. *Biochem. Soc. Trans.* 33:1250–1253. http://dx.doi.org/10.1042/BST20051250

Dhand, R., K. Hara, I. Hiles, B. Bax, I. Gout, G. Panayotou, M.J. Fry, K. Yonezawa, M. Kasuga, and M.D. Waterfield. 1994. PI 3-kinase: Structural and functional analysis of intersubunit interactions. *EMBO J.* 13:511–521.

Döbereiner, H.G., B.J. Dubin-Thaler, J.M. Hofman, H.S. Xenias, T.N. Sims, G. Giannone, M.L. Dustin, C.H. Wiggins, and M.P. Sheetz. 2006. Lateral membrane waves constitute a universal dynamic pattern of motile cells. *Phys. Rev. Lett.* 97:038102. http://dx.doi.org/10.1103/PhysRevLett.97.038102

Dunn, G.A., and A.F. Brown. 1987. A unified approach to analysing cell motility. *J. Cell Sci. Suppl.* 8:81–102.

Friedl, P., and K. Wolf. 2010. Plasticity of cell migration: A multiscale tuning model. *J. Cell Biol.* 188:11–19. http://dx.doi.org/10.1083/jcb.200909003

Gail, M.H., and C.W. Boone. 1970. The locomotion of mouse fibroblasts in tissue culture. *Biophys. J.* 10:980–993. http://dx.doi.org/10.1016/S0006-3495(70)86347-0

Giannone, G., B.J. Dubin-Thaler, H.-G. Döbereiner, N. Kieffer, A.R. Bresnick, and M.P. Sheetz. 2004. Periodic lamellipodial contractions correlate with rearward actin waves. *Cell.* 116:431–443. http://dx.doi.org/10.1016/S0092-8674(04)00058-3

Gupton, S.L., K.L. Anderson, T.P. Kole, R.S. Fischer, A. Ponti, S.E. Hitchcock-DeGregori, G. Danuser, V.M. Fowler, D. Wirtz, D. Hanein, and C.M. Waterman-Storer. 2005. Cell migration without a lamellipodium: Translation of actin dynamics into cell movement mediated by tropomyosin. *J. Cell Biol.* 168:619–631. http://dx.doi.org/10.1083/jcb.200406063

Hoeller, O., and R.R. Kay. 2007. Chemotaxis in the absence of PIP3 gradients. *Curr. Biol.* 17:813–817. http://dx.doi.org/10.1016/j.cub.2007.04.004

Laukaitis, C.M., D.J. Webb, K. Donais, and A.F. Horwitz. 2001. Differential dynamics of α5 integrin, paxillin, and α-actinin during formation and disassembly of adhesions in migrating cells. *J. Cell Biol.* 153:1427–1440. http://dx.doi.org/10.1083/jcb.153.7.1427

Lebensohn, A.M., and M.W. Kirschner. 2009. Activation of the WAVE complex by coincident signals controls actin assembly. *Mol. Cell.* 36:512–524. http://dx.doi.org/10.1016/j.molcel.2009.10.024

Lo, C.-M., D.B. Buxton, G.C.H. Chua, M. Dembo, R.S. Adelstein, and Y.-L. Wang. 2004. Nonmuscle myosin IIb is involved in the guidance of fibroblast migration. *Mol. Biol. Cell.* 15:982–989. http://dx.doi.org/10.1091/mbc.E03-06-0359

Loovers, H.M., M. Postma, I. Keizer-Gunnink, Y.E. Huang, P.N. Devreotes, and P.J. van Haastert. 2006. Distinct roles of PI(3,4,5)P3 during chemoattractant signaling in *Dictyostelium*: A quantitative in vivo analysis by inhibition of PI3-kinase. *Mol. Biol. Cell.* 17:1503–1513. http://dx.doi.org/10.1091/mbc.E05-09-0825

Machacek, M., and G. Danuser. 2006. Morphodynamic profiling of protrusion phenotypes. *Biophys. J.* 90:1439–1452. http://dx.doi.org/10.1529/biophysj.105.070383

Machacek, M., L. Hodgson, C. Welch, H. Elliott, O. Pertz, P. Nalbant, A. Abell, G.L. Johnson, K.M. Hahn, and G. Danuser. 2009. Coordination of Rho GTPase activities during cell protrusion. *Nature.* 461:99–103. http://dx.doi.org/10.1038/nature08242

Melvin, A.T., E.S. Welf, Y. Wang, D.J. Irvine, and J.M. Haugh. 2011. In chemotaxing fibroblasts, both high-fidelity and weakly biased cell movements track the localization of PI3K signaling. *Biophys. J.* 100:1893–1901. http://dx.doi.org/10.1016/j.bpj.2011.02.047

Merlot, S., and R.A. Firtel. 2003. Leading the way: Directional sensing through phosphatidylinositol 3-kinase and other signaling pathways. *J. Cell Sci.* 116:3471–3478. http://dx.doi.org/10.1242/jcs.00703

Millius, A., S.N. Dandekar, A.R. Houk, and O.D. Weiner. 2009. Neutrophils establish rapid and robust WAVE complex polarity in an actin-dependent fashion. *Curr. Biol.* 19:253–259. http://dx.doi.org/10.1016/j.cub.2008.12.044

Monypenny, J., D. Zicha, C. Higashida, F. Oceguera-Yanez, S. Narumiya, and N. Watanabe. 2009. Cdc42 and Rac family GTPases regulate mode and speed but not direction of primary fibroblast migration during platelet-derived growth factor-dependent chemotaxis. *Mol. Cell. Biol.* 29:2730–2747. http://dx.doi.org/10.1128/MCB.01285-08

Oikawa, T., H. Yamaguchi, T. Itoh, M. Kato, T. Ijuin, D. Yamazaki, S. Suetsugu, and T. Takenawa. 2004. PtdIns(3,4,5)P3 binding is necessary for WAVE2-induced formation of lamellipodia. *Nat. Cell Biol.* 6:420–426. http://dx.doi.org/10.1038/ncb1125

Pankov, R., Y. Endo, S. Even-Ram, M. Araki, K. Clark, E. Cukierman, K. Matsumoto, and K.M. Yamada. 2005. A Rac switch regulates random versus directionally persistent cell migration. *J. Cell Biol.* 170:793–802. http://dx.doi.org/10.1083/jcb.200503152

Petrie, R.J., A.D. Doyle, and K.M. Yamada. 2009. Random versus directionally persistent cell migration. *Nat. Rev. Mol. Cell Biol.* 10:538–549. http://dx.doi.org/10.1038/nrm2729

Ponti, A., M. Machacek, S.L. Gupton, C.M. Waterman-Storer, and G. Danuser. 2004. Two distinct actin networks drive the protrusion of migrating cells. *Science.* 305:1782–1786. http://dx.doi.org/10.1126/science.1100533

Postma, M., J. Roelofs, J. Goedhart, T.W.J. Gadella, A.J.W.G. Visser, and P.J.M. Van Haastert. 2003. Uniform cAMP stimulation of *Dictyostelium* cells induces localized patches of signal transduction and pseudopodia. *Mol. Biol. Cell*. 14:5019–5027. http://dx.doi.org/10.1091/mbc.E03-08-0566

Ridley, A.J., M.A. Schwartz, K. Burridge, R.A. Firtel, M.H. Ginsberg, G. Borisy, J.T. Parsons, and A.R. Horwitz. 2003. Cell migration: Integrating signals from front to back. *Science*. 302:1704–1709. http://dx.doi.org/10.1126/science.1092053

Riedl, J., A.H. Crevenna, K. Kessenbrock, J.H. Yu, D. Neukirchen, M. Bista, F. Bradke, D. Jenne, T.A. Holak, Z. Werb, et al. 2008. Lifeact: A versatile marker to visualize F-actin. *Nat. Methods*. 5:605–607. http://dx.doi.org/10.1038/nmeth.1220

Sabouri-Ghomi, M., Y. Wu, K. Hahn, and G. Danuser. 2008. Visualizing and quantifying adhesive signals. *Curr. Opin. Cell Biol.* 20:541–550. http://dx.doi.org/10.1016/j.ceb.2008.05.004

Sasaki, A.T., C. Janetopoulos, S. Lee, P.G. Charest, K. Takeda, L.W. Sundheimer, R. Meili, P.N. Devreotes, and R.A. Firtel. 2007. G protein–independent Ras/PI3K/F-actin circuit regulates basic cell motility. *J. Cell Biol.* 178:185–191. http://dx.doi.org/10.1083/jcb.200611138

Schneider, I.C., and J.M. Haugh. 2004. Spatial analysis of 3′ phosphoinositide signaling in living fibroblasts: II. Parameter estimates for individual cells from experiments. *Biophys. J.* 86:599–608. http://dx.doi.org/10.1016/S0006-3495(04)74138-7

Schneider, I.C., and J.M. Haugh. 2005. Quantitative elucidation of a distinct spatial gradient-sensing mechanism in fibroblasts. *J. Cell Biol.* 171:883–892. http://dx.doi.org/10.1083/jcb.200509028

Schneider, I.C., E.M. Parrish, and J.M. Haugh. 2005. Spatial analysis of 3′ phosphoinositide signaling in living fibroblasts, III: Influence of cell morphology and morphological Polarity. *Biophys. J.* 89:1420–1430. http://dx.doi.org/10.1529/biophysj.105.061218

Sossey-Alaoui, K., X.R. Li, T.A. Ranalli, and J.K. Cowell. 2005. WAVE3-mediated cell migration and lamellipodia formation are regulated downstream of phosphatidylinositol 3-kinase. *J. Biol. Chem.* 280:21748–21755. http://dx.doi.org/10.1074/jbc.M500503200

Swaney, K.F., C.H. Huang, and P.N. Devreotes. 2010. Eukaryotic chemotaxis: A network of signaling pathways controls motility, directional sensing, and polarity. *Annu Rev Biophys*. 39:265–289. http://dx.doi.org/10.1146/annurev.biophys.093008.131228

Takeda, K., A.T. Sasaki, H.J. Ha, H.A. Seung, and R.A. Firtel. 2007. Role of phosphatidylinositol 3-kinases in chemotaxis in *Dictyostelium*. *J. Biol. Chem.* 282:11874–11884. http://dx.doi.org/10.1074/jbc.M610984200

Tsukada, Y., K. Aoki, T. Nakamura, Y. Sakumura, M. Matsuda, and S. Ishii. 2008. Quantification of local morphodynamics and local GTPase activity by edge evolution tracking. *PLOS Comput. Biol.* 4:e1000223. http://dx.doi.org/10.1371/journal.pcbi.1000223

Uetrecht, A.C., and J.E. Bear. 2009. Golgi polarity does not correlate with speed or persistence of freely migrating fibroblasts. *Eur. J. Cell Biol.* 88:711–717. http://dx.doi.org/10.1016/j.ejcb.2009.08.001

Van Haastert, P.J. 2010. A stochastic model for chemotaxis based on the ordered extension of pseudopods. *Biophys. J.* 99:3345–3354. http://dx.doi.org/10.1016/j.bpj.2010.09.042

van Haastert, P.J., and M. Postma. 2007. Biased random walk by stochastic fluctuations of chemoattractant-receptor interactions at the lower limit of detection. *Biophys. J.* 93:1787–1796. http://dx.doi.org/10.1529/biophysj.107.104356

Van Haastert, P.J.M., and P.N. Devreotes. 2004. Chemotaxis: Signalling the way forward. *Nat. Rev. Mol. Cell Biol.* 5:626–634. http://dx.doi.org/10.1038/nrm1435

Vicente-Manzanares, M., J. Zareno, L. Whitmore, C.K. Choi, and A.F. Horwitz. 2007. Regulation of protrusion, adhesion dynamics, and polarity by myosins IIA and IIB in migrating cells. *J. Cell Biol.* 176:573–580. http://dx.doi.org/10.1083/jcb.200612043

Vicente-Manzanares, M., C.K. Choi, and A.R. Horwitz. 2009. Integrins in cell migration—the actin connection. *J. Cell Sci.* 122:199–206. http://dx.doi.org/10.1242/jcs.018564

Ware, M.F., A. Wells, and D.A. Lauffenburger. 1998. Epidermal growth factor alters fibroblast migration speed and directional persistence reciprocally and in a matrix-dependent manner. *J. Cell Sci.* 111:2423–2432.

Weiger, M.C., C.-C. Wang, M. Krajcovic, A.T. Melvin, J.J. Rhoden, and J.M. Haugh. 2009. Spontaneous phosphoinositide 3-kinase signaling dynamics drive spreading and random migration of fibroblasts. *J. Cell Sci.* 122:313–323. http://dx.doi.org/10.1242/jcs.037564

Weiger, M.C., S. Ahmed, E.S. Welf, and J.M. Haugh. 2010. Directional persistence of cell migration coincides with stability of asymmetric intracellular signaling. *Biophys. J.* 98:67–75. http://dx.doi.org/10.1016/j.bpj.2009.09.051

Weiner, O.D., W.A. Marganski, L.F. Wu, S.J. Altschuler, and M.W. Kirschner. 2007. An actin-based wave generator organizes cell motility. *PLoS Biol.* 5:e221. http://dx.doi.org/10.1371/journal.pbio.0050221

Wu, Y.I., D. Frey, O.I. Lungu, A. Jaehrig, I. Schlichting, B. Kuhlman, and K.M. Hahn. 2009. A genetically encoded photoactivatable Rac controls the motility of living cells. *Nature*. 461:104–108. http://dx.doi.org/10.1038/nature08241

Xiong, Y., C.H. Huang, P.A. Iglesias, and P.N. Devreotes. 2010. Cells navigate with a local-excitation, global-inhibition-biased excitable network. *Proc. Natl. Acad. Sci. USA*. 107:17079–17086. http://dx.doi.org/10.1073/pnas.1011271107

Yoo, S.K., Q. Deng, P.J. Cavnar, Y.I. Wu, K.M. Hahn, and A. Huttenlocher. 2010. Differential regulation of protrusion and polarity by PI3K during neutrophil motility in live zebrafish. *Dev. Cell*. 18:226–236. http://dx.doi.org/10.1016/j.devcel.2009.11.015